ERC-Zarathustra: Advances in electrodeless plasma thruster modeling, experiments, and data-driven analysis

Mario Merino, Davide Maddaloni, Célian Boyé, Diego García-Lahuerta, Matteo Ripoli, Borja Bayón-Buján, Pedro Jiménez, Filippo Terragni, Jaume Navarro-Cavallé, Pablo Fajardo, Eduardo Ahedo

2023 EPIC Workshop, May 9-12 2023, Naples, Italy

Contents

Magnetic arch experimental study

MAT2 sources under assembly

- **EPTs** have a net magnetic dipole that will produce a secular torque in the geomagnetic field
- A tandem of two EPTs with opposing polarity cancels the net dipole
- The magnetic nozzles interact forming a new topology for plasma expansion, the 'Magnetic arch'
- New, exotic EPT designs like the U-thruster also feature a 'Magnetic arch'

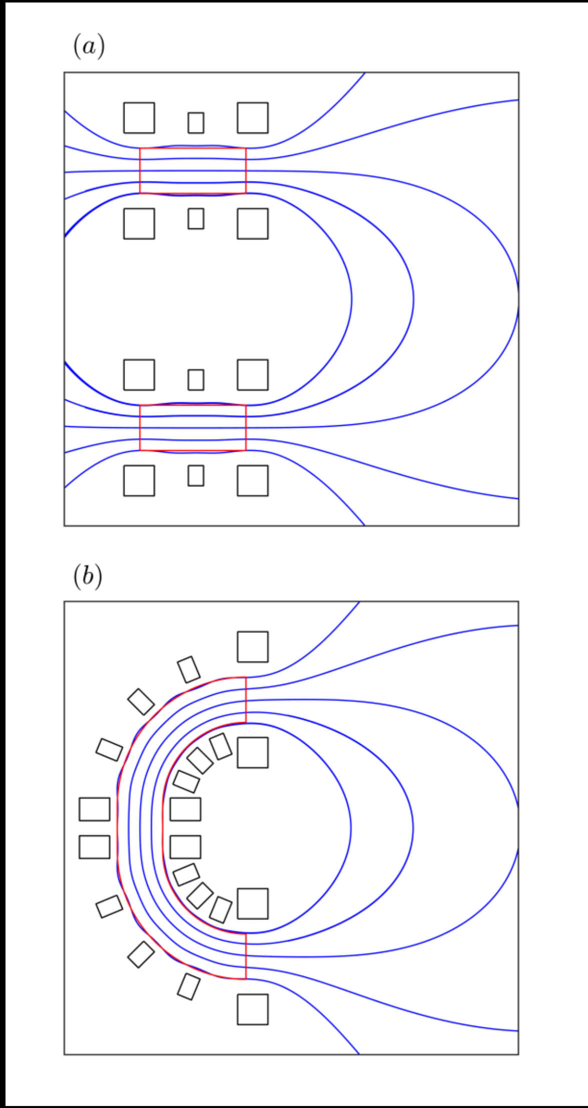

Experimental Setup

Electromagnets	
Maximum total power per source	1 kW
Maximum magnetic field intensity	900 G
ECR resonance field	875 G
Total number of turns per source	≈ 1200

Ionisation chamber	
Length	50 mm
Diameter	30 mm
Material	Non-magnetic Stainless Steel

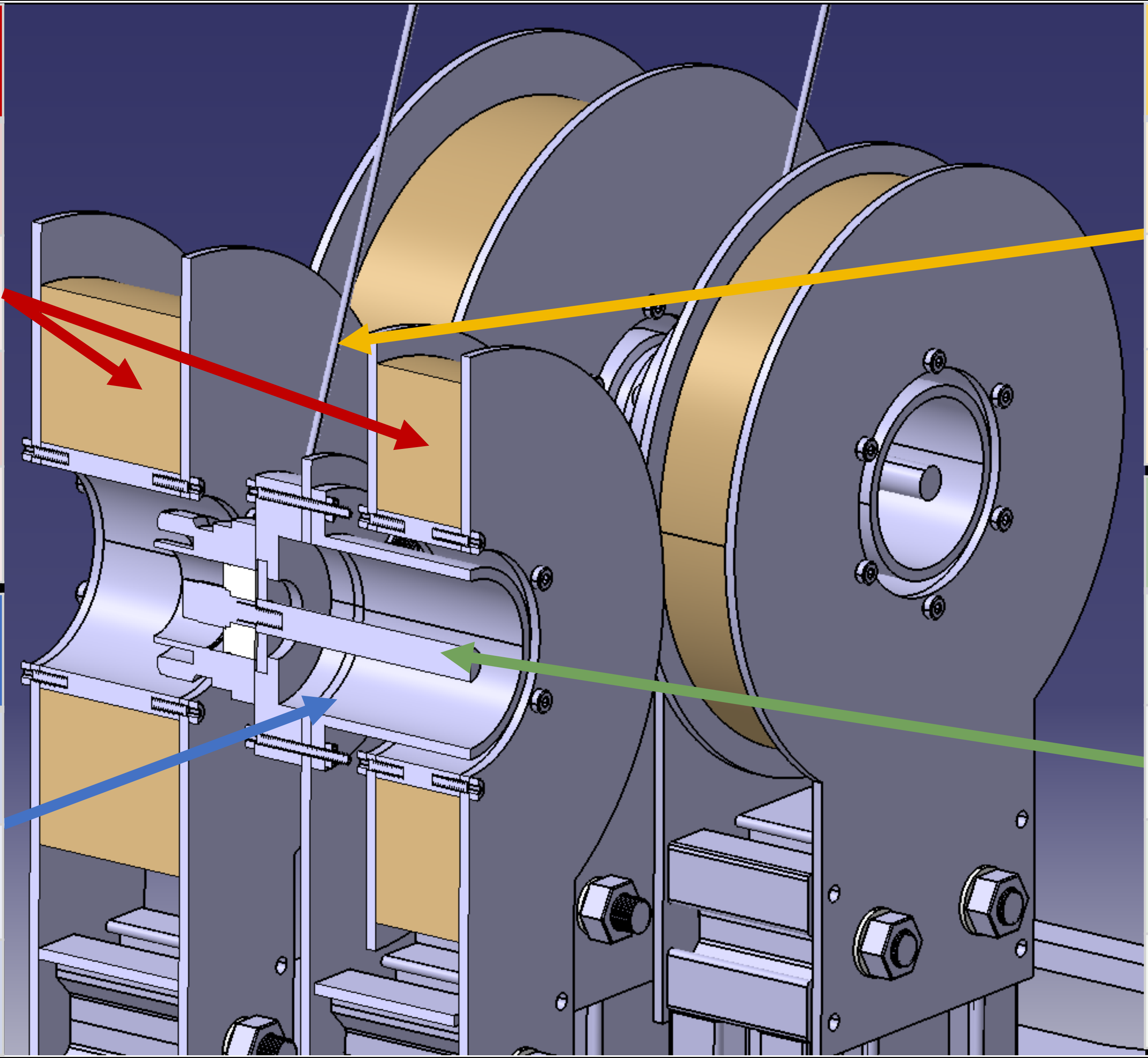

Gas feeding	
Gas	Krypton
Ignition mass flow rate	50 sccm
Operation mass flow rate	15 sccm

Inductor	
Length	50 mm
Diameter	6 mm
Frequency	2.45 GHz
Power	50 W–500 W

Experimental Setup

- Two magnetic topologies have been characterized.

*Magnetic field with "**MF ARCH**" configuration.*

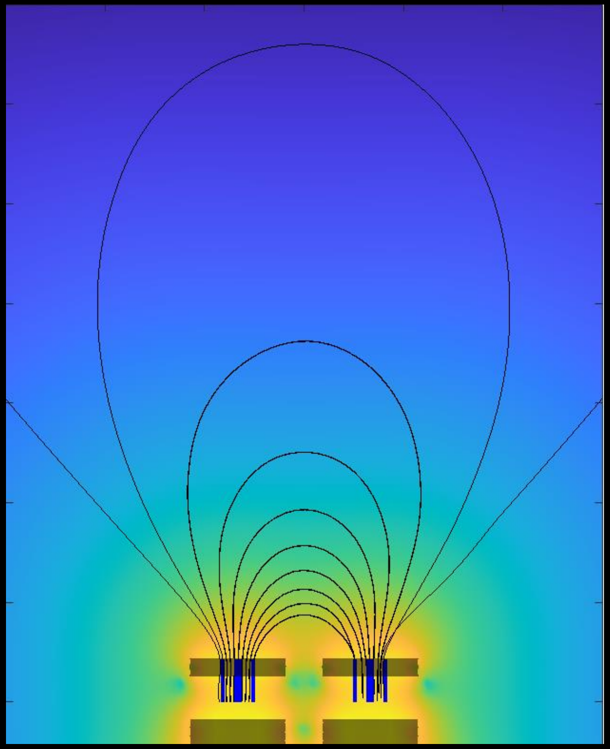

*Magnetic field with "**MF SP**" configuration.*

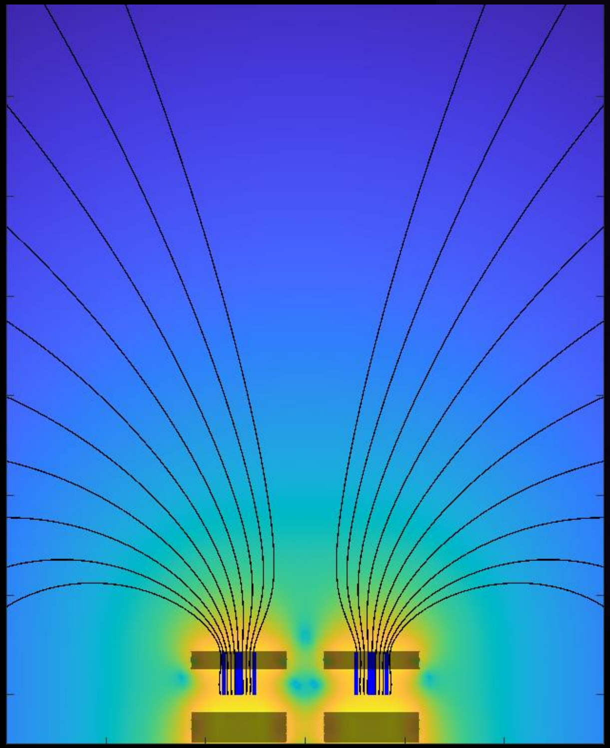

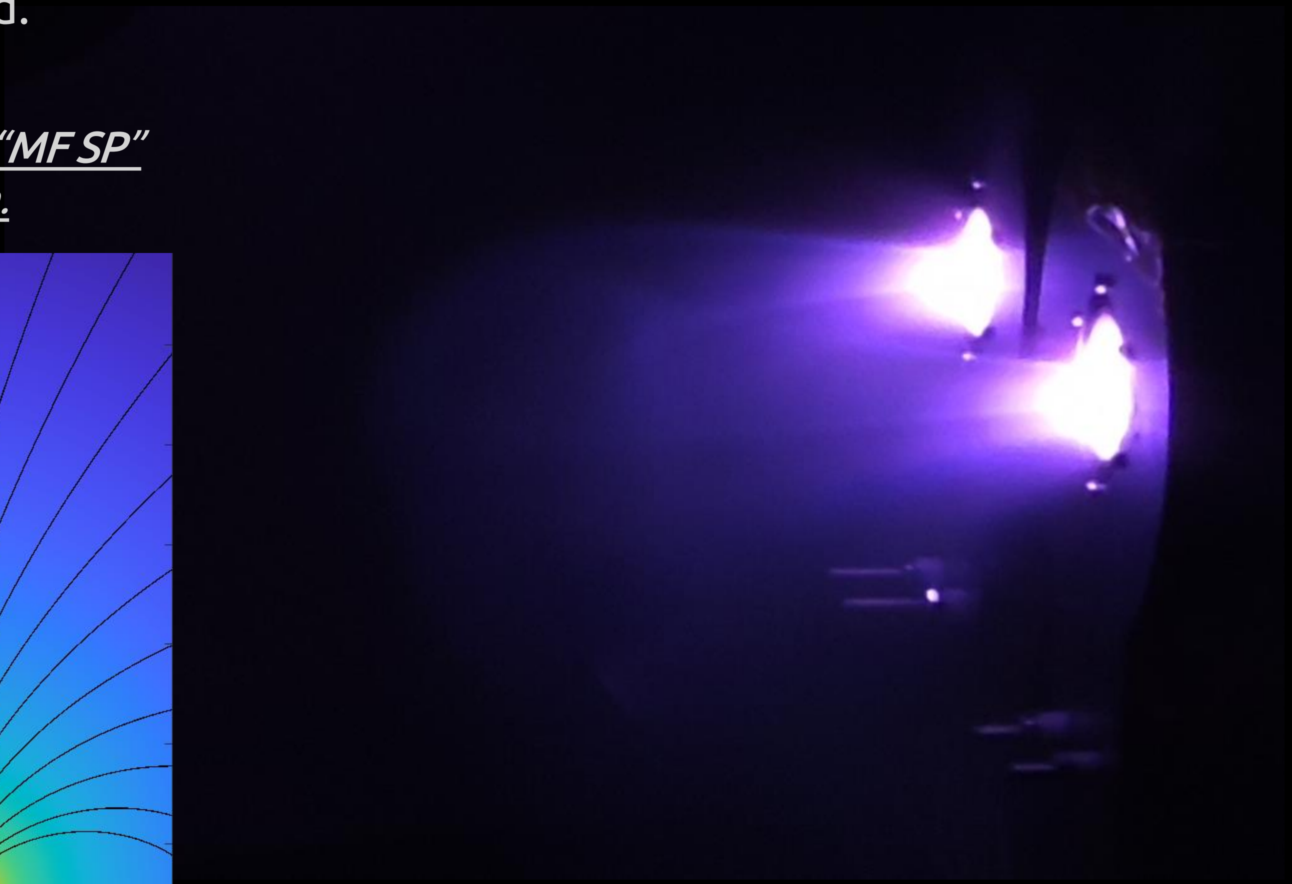

*Thruster in operation with Krypton in **MF ARCH** configuration.*

Results - Ion Flux

- Ion current density computed from RPA data at 38 cm from exit plane
- In spite of the closed magnetic lines, the plasma can form an ion beam that expands freely beyond the magnetic arch
- Ion energy depends on area expansion ratio, which is different in the three configuration (lower for arch configuration, partially due to lower plume divergence angle)

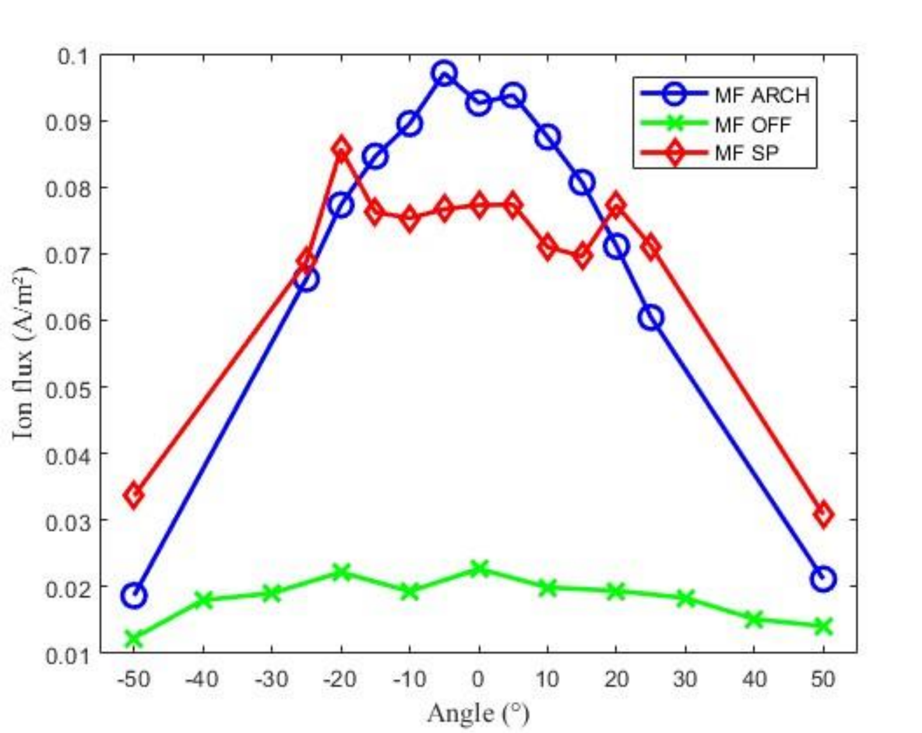

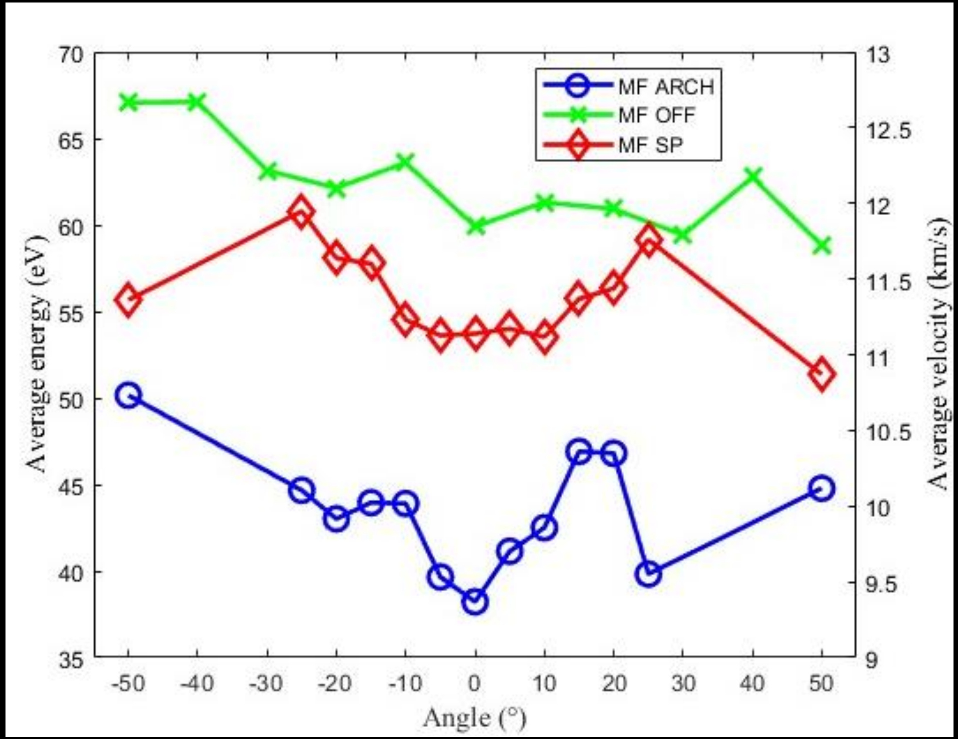

Magnetic arch simulation study

- Two-fluid (ion, electron), quasineutral, collisionless 2D planar simulation
- 1st order Discontinuous Galerkin on unstructured mesh

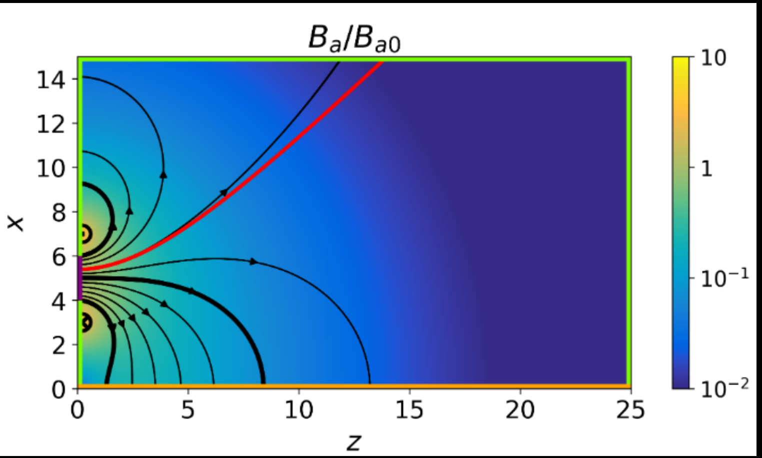

- Free ion beam in spite of the closed magnetic lines
- Formation of oblique, collisionless shock
- Large electron current in outermost ("open") lines to satisfy current-free condition
- Positive magnetic thrust generation (albeit small drag contribution downstream)

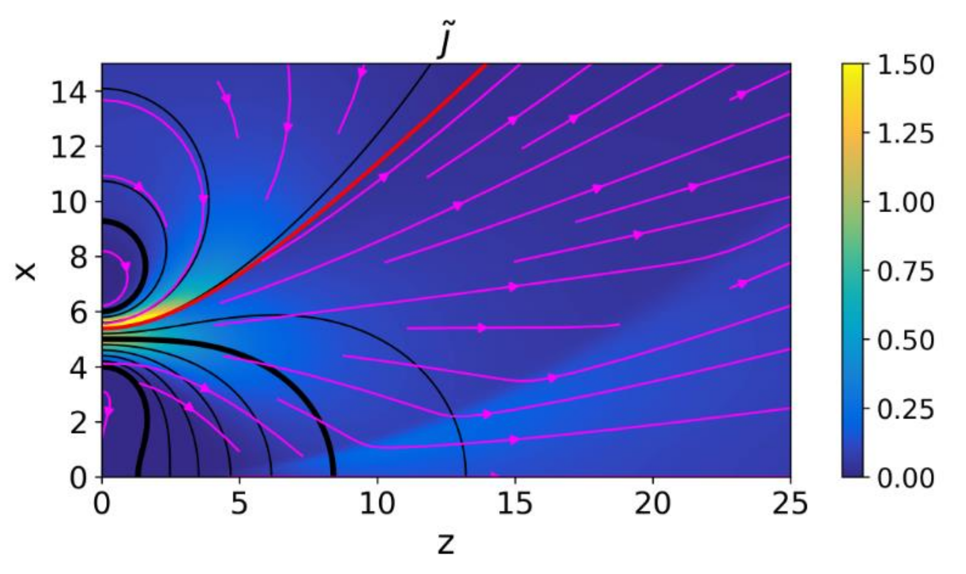

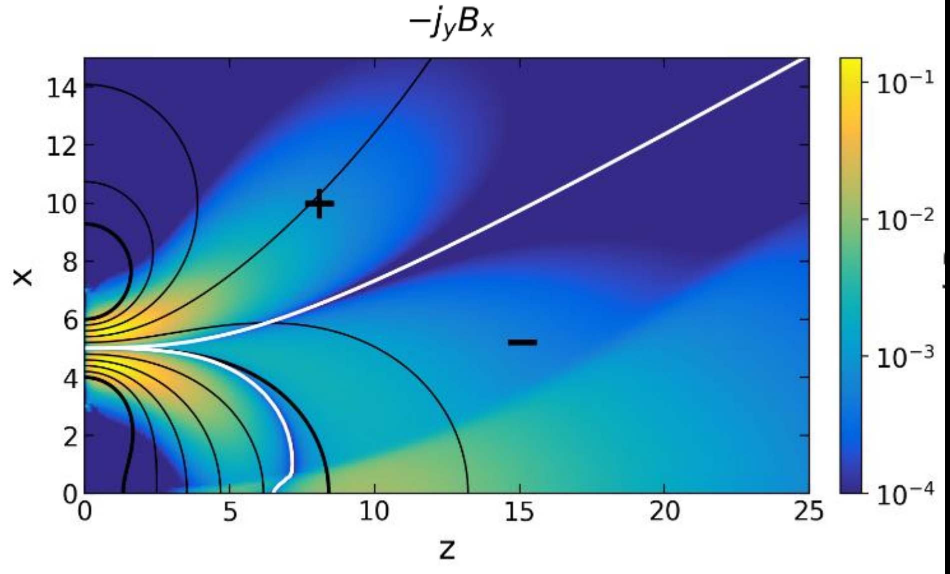

Magnetic arch simulation study

- Importance of the plasma-induce magnetic field:
  - “Stretches” the magnetic arch downstream
  - Generates new magnetic region, disconnected from the source
  - Lowers the drag contribution to magnetic thrust → Larger thrust

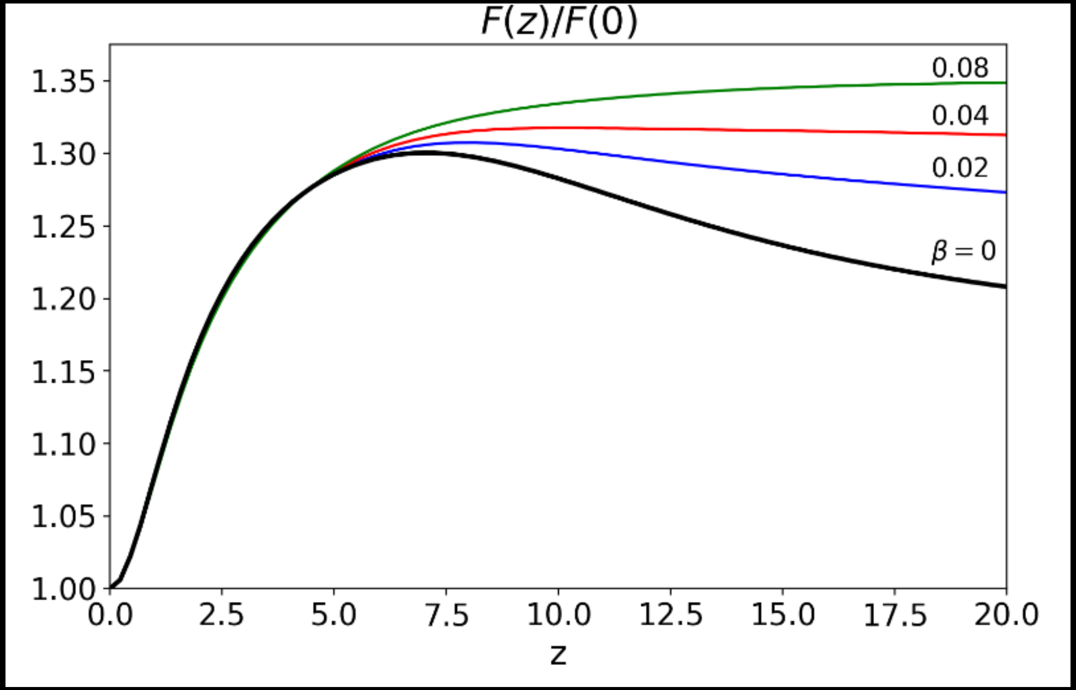

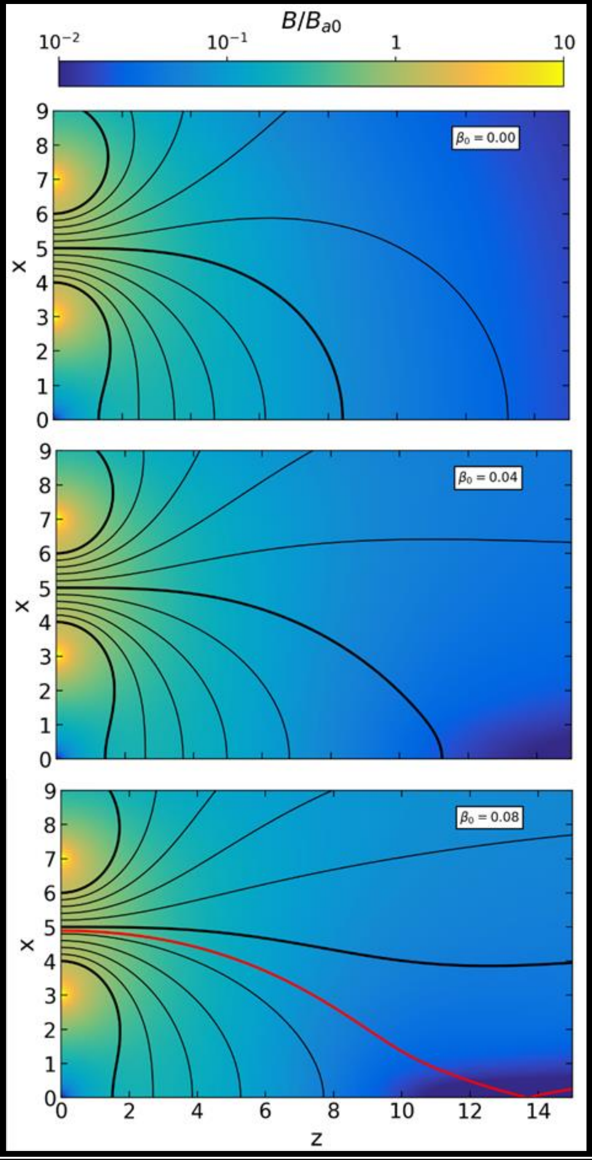

Analytic study of drift wave dispersion relation

- A magnetic nozzle is a slowly-diverging quasi-collisionless plasma column with flux
- Azimuthal waves exist. Some may become unstable (e.g. Simon-Hoh instability)
- Work in progress, derivation and characterization of simple yet relevant dispersion relations

$$k^2\rho_e^2\frac{\omega_{LH}^2}{\omega_i^2} \simeq \frac{\omega_D - \omega_B + k^2\rho_e^2(\omega_e + i\nu_\perp) - (2\omega_B)\left(\frac{2\omega_e + \omega_D - \omega_B}{2\omega_{ce}}\right)^2 - \frac{k_z^2 c_e^2}{\omega_e + \omega_D - \omega_B + i\nu_\parallel}}{\omega_e + \omega_D - \omega_B + ik^2\rho_e^2\nu_\perp - (\omega_e + 2\omega_B)\left(\frac{2\omega_e + \omega_D - \omega_B}{2\omega_{ce}}\right)^2 - \frac{k_z^2 c_e^2}{\omega_e + \omega_D - \omega_B + i\nu_\parallel}}$$

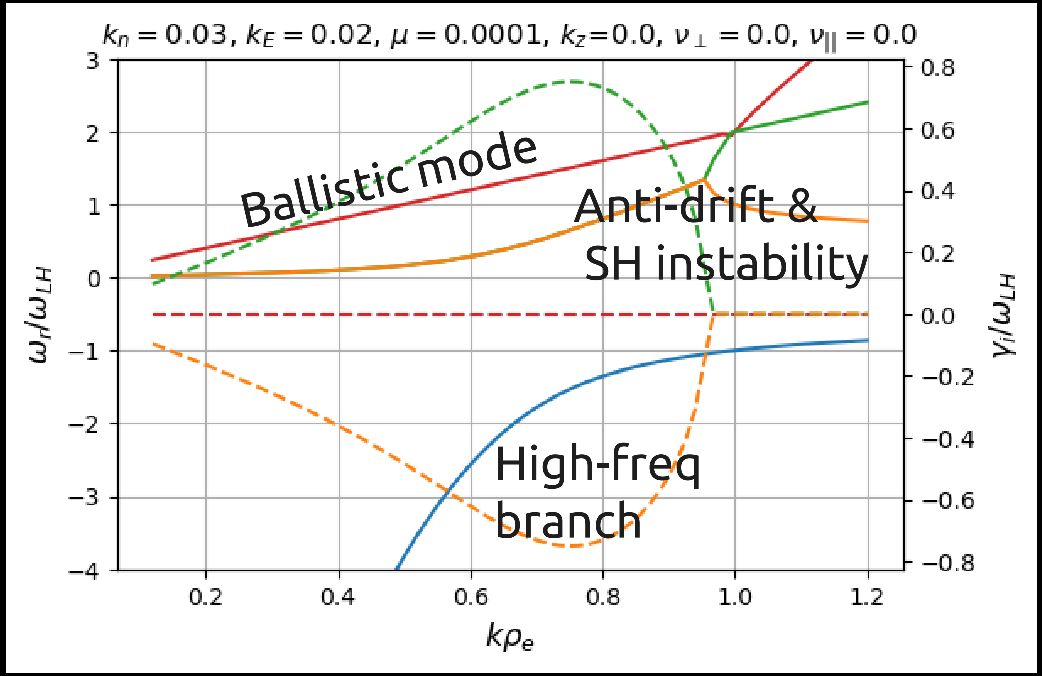

With collisions and k_z

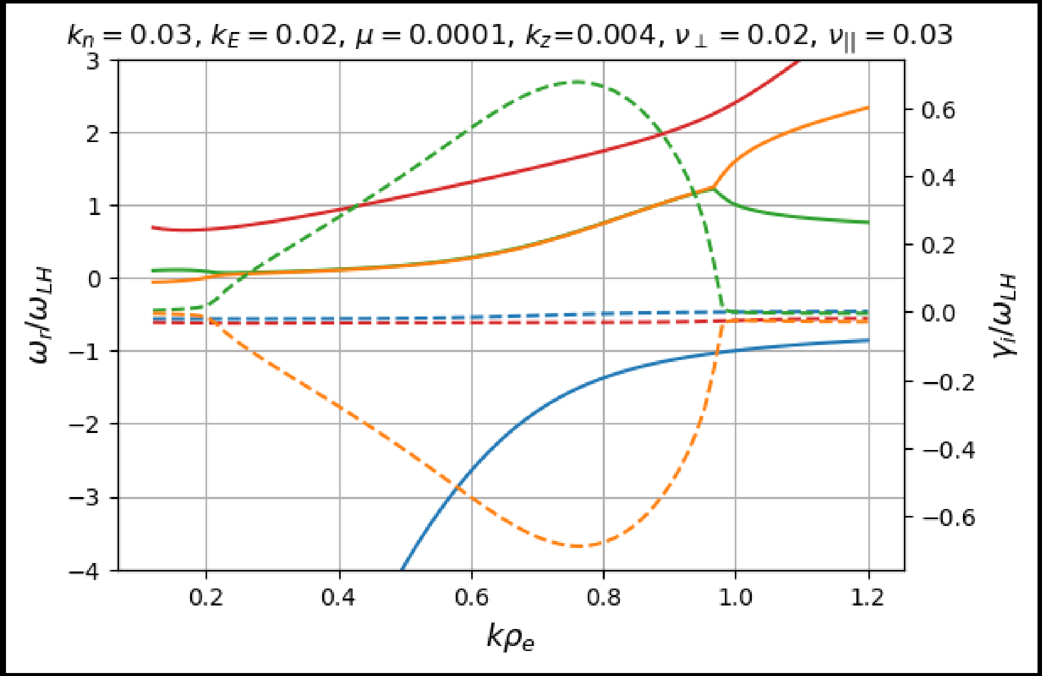

Drift wave measurements in MN

- Ongoing work with 3 probes operating in floating mode to characterize spatiotemporal oscillations in the MN of a helicon plasma thruster

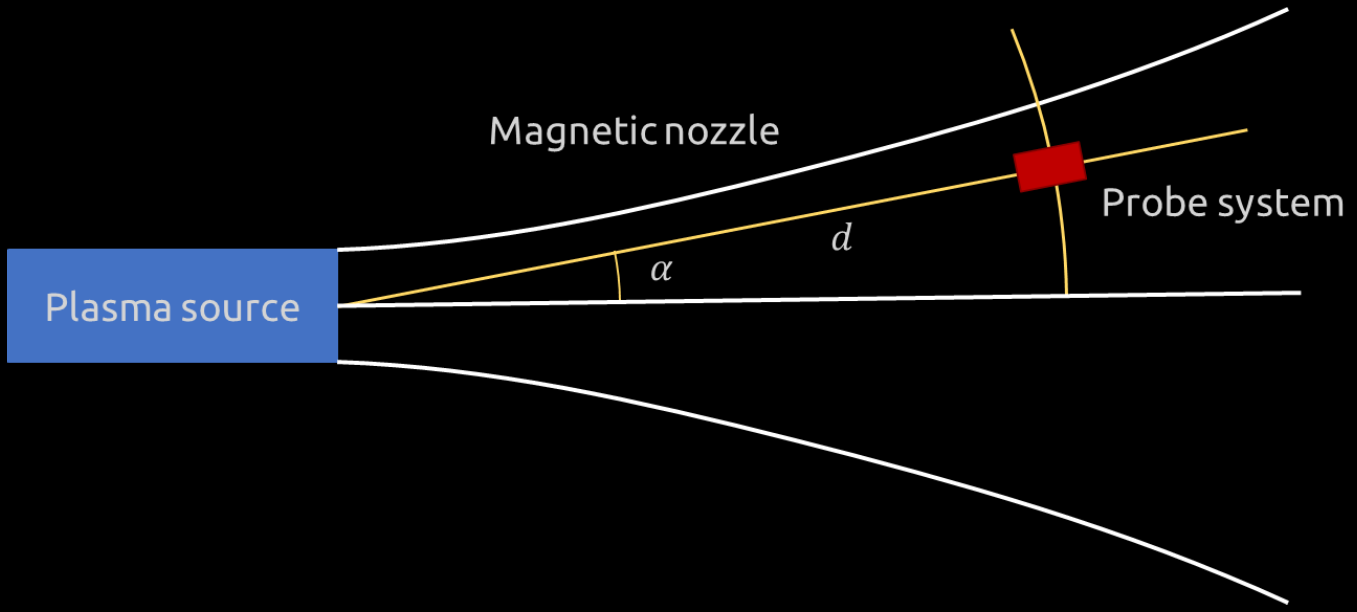

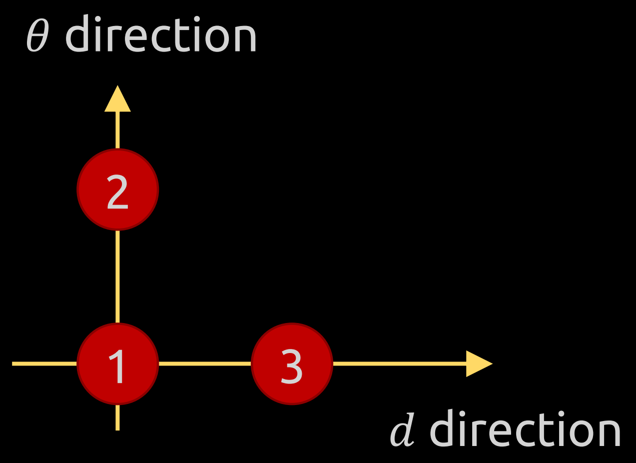

Drift wave measurements in MN

- Cross-correlation allows identifying, for each frequency:
  - Mean phase difference and standard deviation → wave number k
  - Correlated power magnitude
- Example at $d = 100$ mm, $\alpha = 35$ deg:
  - Local maximum of power at ~55 kHz
  - Azimuthal dispersion relation in the $\nabla n \times \boldsymbol{B}$ drift direction
  - Small/non existant k in the d direction

Power

θ direction

d direction

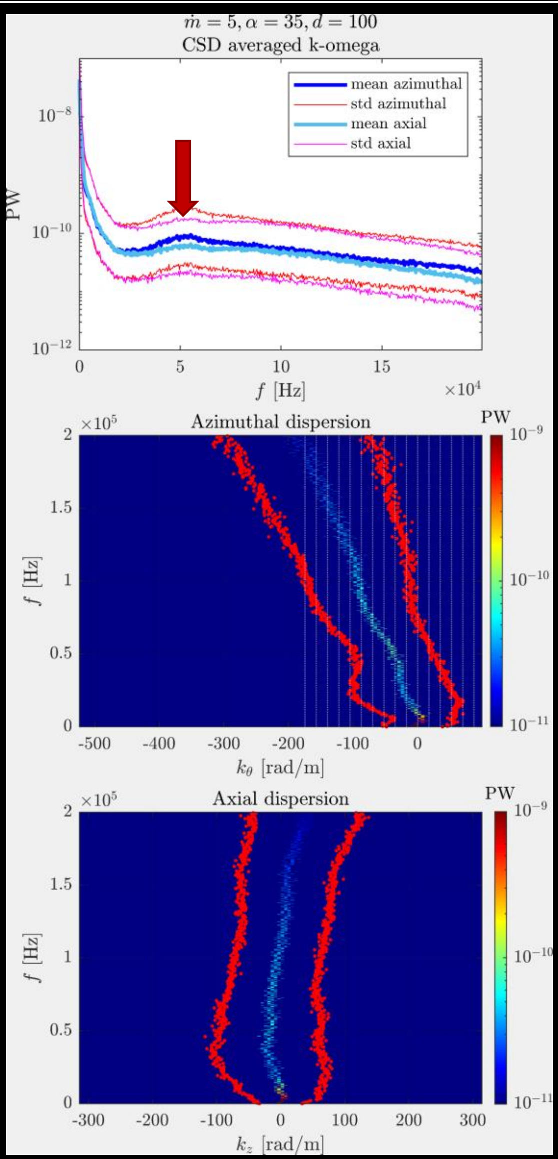

Symbolic regression of breathing mode in HETs

- Physics-informed data driven analysis using SINDy and variants: knowledge about the physics can be used in the process (to limit search and to select valid models)
- Data from HYPHEN simulations of HET discharge, featuring an evident breathing mode
- Models of different degrees of complexity/fidelity can be obtained
  - E.g. mean density in the ionization region:

```
MODEL1. Self-consistent model for ni, nn:
[0.95] [0.00] ni_dot = + -1.41e+05 ni + 3.97e-14 ni nn
[0.94] [0.00] nn_dot = + 4.51e+04 nn + -4.79e-14 ni nn
----------------------------------
MODEL2. Model for ni, nn; Rion(Te) as input:
[0.87] [0.00] ni_dot = + -2.26e+05 ni + 4.67e-15 ni nn Rion(Te)
[0.84] [0.00] nn_dot = + 1.77e+23 1 + -3.50e-15 ni nn Rion(Te)
----------------------------------
MODEL3. Model for ni, nn; Rion(Te), ui_z as inputs:
[0.95] [0.00] ni_dot = + -4.12e+01 ni ui_z + 8.16e-01 ni nn Rion(Te)
[0.88] [0.00] nn_dot = + 1.83e+23 1 + -7.68e-01 ni nn Rion(Te)
----------------------------------
```

Analogous to Fife's predator-prey model:

$$\begin{cases} \dfrac{\partial n_i}{\partial t} = -\dfrac{u_i}{L} n_i + \xi n_n n_i \\ \dfrac{\partial n_n}{\partial t} = \dfrac{u_n}{L} n_n - \xi n_n n_i \end{cases}$$

But with physically-sound neutral injection term and ionization term

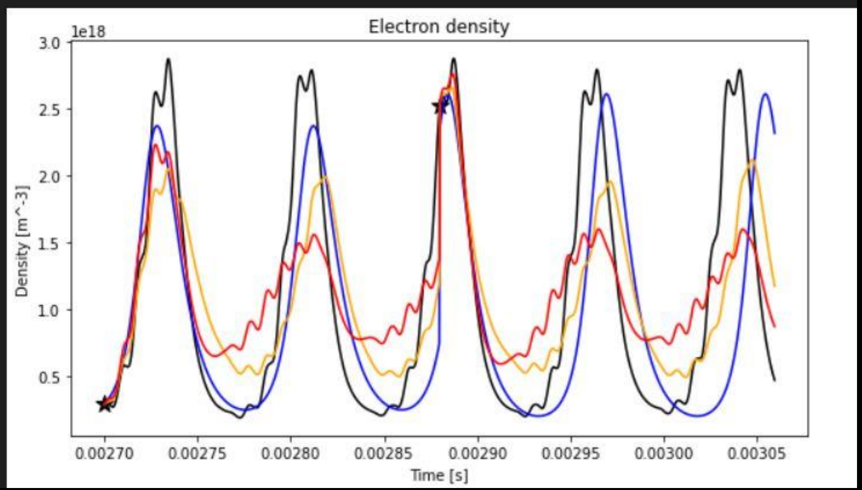

- Integrated models reproduce oscillations for a limited period of time (e.g. models decay).
  - Work in progress: increase fidelity of model to larger time windows

Symbolic regression of breathing mode in HETs

- Local regression analysis identifies channel regions of behavioral change
  - Near the walls, recombination modifies the model structure
  - Upstream/downstream breathing mode physics are different
- Model score in the channel shows where simple models begin to fail

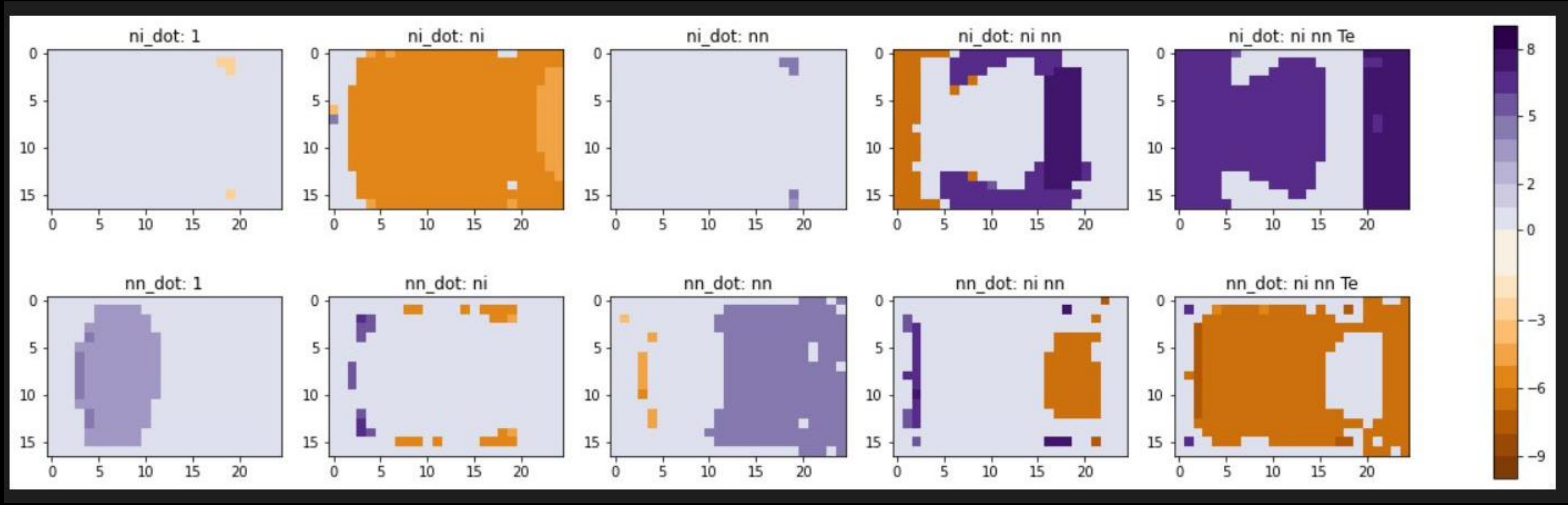

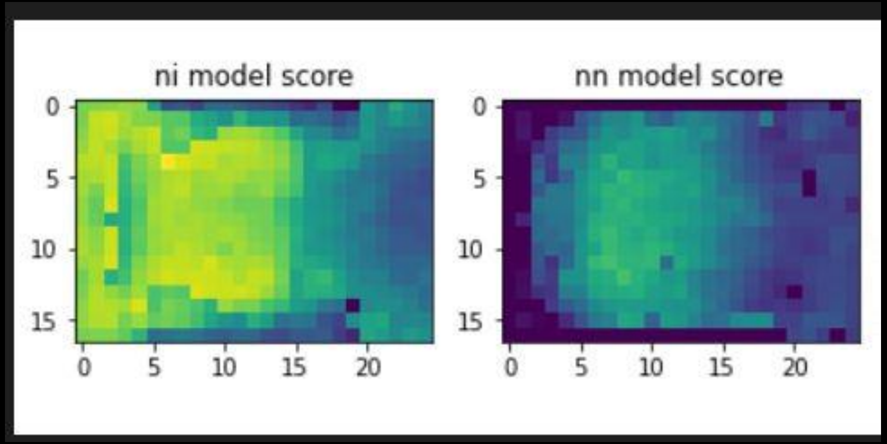

Implicit Particle-in-Cell Algorithm

- Time-implicit → breaks λ_{De} and ω_{pe} constraints
  - Cell size and time step can be larger than in explicit PIC
- Exactly global-energy and local-charge conserving
- Advanced boundary conditions for injection and free space
- Adaptive mesh
- Optimized orbit – suborbit – segment hierarchy in the particle mover
- Currently electrostatic and quasi-1D (useful for magnetic nozzle expansions)
- Linear time scaling with particles/cell and number of cells
- Speed up of $O(10)$ with respect to explicit PIC

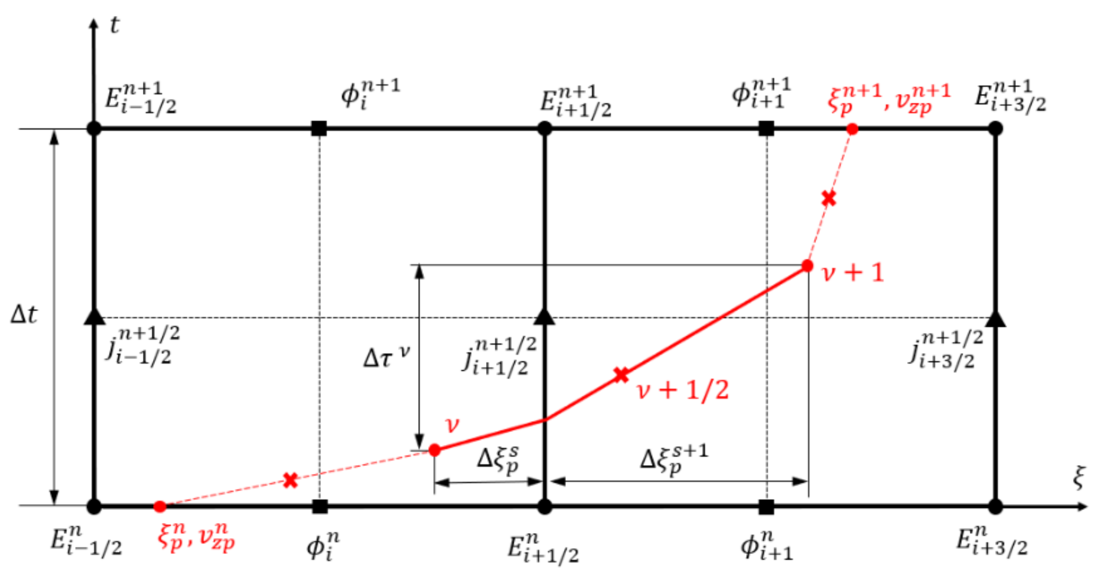

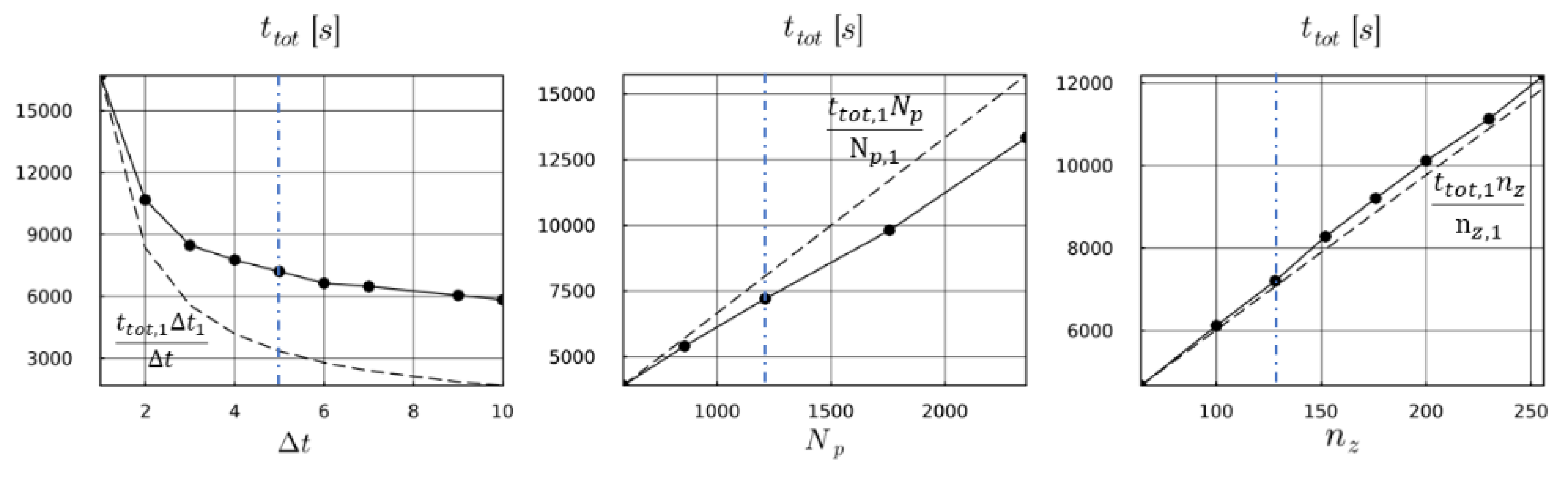

Collaboration with
Luis Chacón, LANL

Implicit Particle-in-Cell Algorithm

- Application to a slowly-diverging magnetic nozzle
  - $O(30)$ faster than state-of-the-art previous work
  - Code correctly reproduces ϕ, n_e, collisionless electron cooling, and fractions of free, reflected, and trapped electrons in the plume

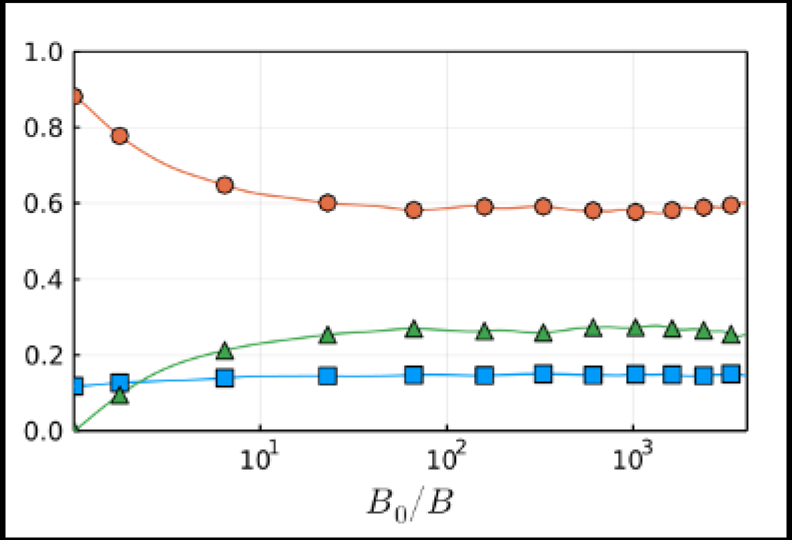

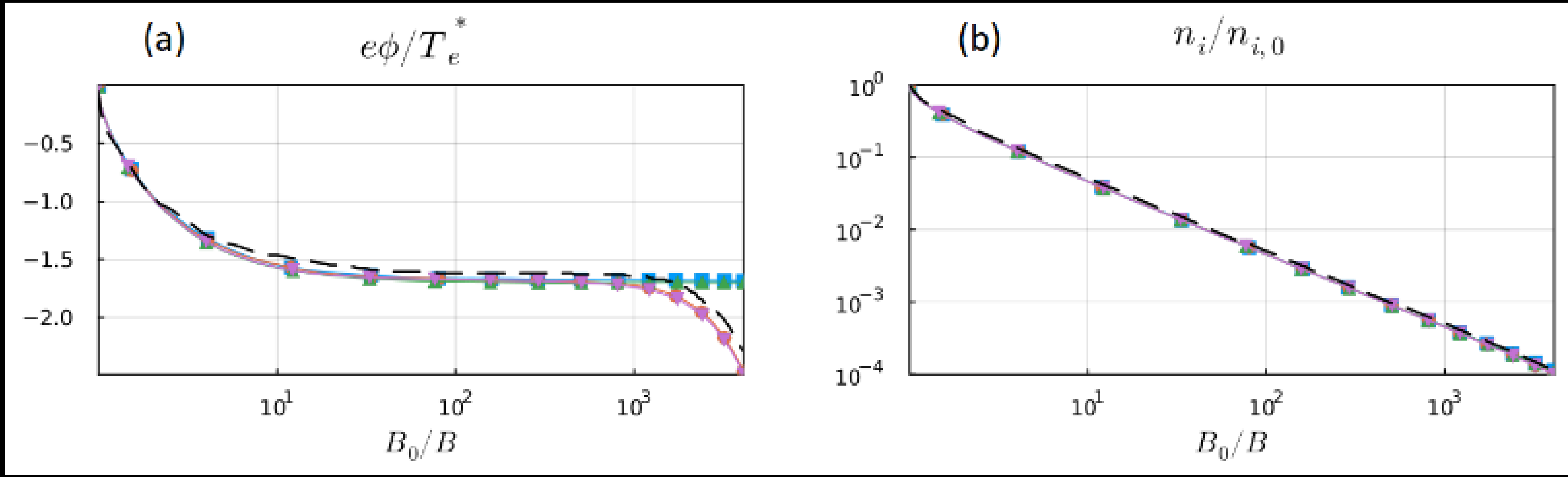

Acknowledgments

This project has received funding from the European Research Council (ERC) under the European Union's Horizon 2020 research and innovation programme (grant agreement No 950466)

European Research Council
Established by the European Commission

Thank you!

mario.merino@uc3m.es

ZARATHUSTRA